RESEARCH ARTICLE

Selection of Magnet Wire Topologies With Reduced AC Losses for the Windings of Electric Drivetrains

AHMED SELEMA[1,2,3], (Member, IEEE), MEHMET GULEC[1,2], MOHAMED N. IBRAHIM[1,2,4],
RUUD SPRANGERS[5], AND PETER SERGEANT[1,2], (Senior Member, IEEE)

[1]Department of Electromechanical, Systems, and Metal Engineering, Ghent University, 9000 Ghent, Belgium
[2]FlandersMake@UGent, Core Laboratory EEDT-MP, 3001 Leuven, Belgium
[3]Department of Electrical Engineering, Faculty of Engineering, Menoufia University, Menoufia 32511, Egypt
[4]Department of Electrical Engineering, Kafrelshiekh University, Kafrelshiekh 33511, Egypt
[5]Punch Powertrain nv, 3800 Sint-Truiden, Belgium

Corresponding author: Ahmed Selema (ahmed.selema@ugent.be)

ABSTRACT In high speed electrical machines, one of the main challenges that can be faced is the high frequency losses in the machine windings due to both skin and proximity effects. This paper studies the effect of using different types of magnet wires on the AC losses in the winding of high speed electric machines. Using finite element modelling (FEM), the conductors are subdivided into multiple strands to calculate the losses in each conductor and in each layer. Aiming at loss minimization, different arrangements are introduced and compared at a wide range of frequencies. Further, four coil designs are prototyped using different magnet wires or arrangements. Moreover, the design and performance are compared with highlighting the pros and cons of each case. Eventually, recommendations are provided based on the obtained results for a better selection of magnet wire.

INDEX TERMS AC losses, electric machines, electromagnetics, magnet wires, skin & proximity effects.

I. INTRODUCTION

This Nowadays, clean transportation is vital for the fight against climate change. Also, the conventional fossil-fuel-powered motors are being replaced by zero-carbon green energy systems. That is why the industrial sector is highly interested in solutions for transportation electrification and sustainable electric mobility. The challenging characteristics of electric vehicles (EVs), such as driving range and charging times are rapidly changing. These improvements depends mainly on efficiency and energy density of the electric powertrain. To this aim, innovation and development of energy efficient electric machines is growing remarkably.

One of the main components that defines the electrical loading capacity in the design of electrical machines is the magnet wire, which is the enameled conductor used for the machine windings. Recently, many manufacturers are deeply

The associate editor coordinating the review of this manuscript and approving it for publication was Kan Liu.

interested in studying different types of wires to guarantee the design of high-efficiency machines with longer lifetime and reduced size and weight. For instance, bad selection of wires or even random allocation of conductors inside the slots could cause an excessive amount of losses as well as poor fill factor. Therefore, coil manufacturing with high reliability and economic efficiency is necessary [1].

High speed electrical machines have been identified as key technologies for EVs applications. In these types of machines, high frequency currents, with fundamental frequencies up to 1kHz, or even higher, pass through the conductors resulting in additional losses due to skin and proximity effects. This most likely appears in the open or semi-closed slot geometry, particularly for the conductors near the slot opening because they are exposed to high leakage flux [1], [2], [3].

Many approaches have been used to estimate the eddy current losses in the machine conductors including skin and proximity losses. Table 1 presents an up-to-date list of recent

TABLE 1. State-of-the-art in the evaluation of AC winding losses.

Ref.	Magnet wire topologies	Method	Frequency range	Application
[4]	Round and Litz wire	Analytical	800 Hz	PM starter generator
[5]	Flat rectangular wire	FEA	50-500 Hz	Fractional slot concentrated winding (FSCW)
[6]	rectangular & stranded wires	FEA	$10 - 10^4$ Hz	Interior PM Synchronous Machine (IPMSM)
[7]	Stranded wire	FEA & Analytical	666.67 Hz	IPMSM
[8]	Multi-strand round-wire	Analytical & experimental	0-500 Hz	IPMSM
[9]	Flat wire	FEA & experimental	0-1000 Hz	High speed PM machines with form-wound windings
[10]	Round wire	Analytical & experimental	0-1333.3 Hz	Slotless PM machines with concentrated winding
[11]	Flat rectangular wire	Analytical & experimental	10 kHz, 20 kHz	Air-Cored Axial Flux PM Machine

Extruded Litz Wire (Type-1)   Profiled Litz Wire (Type-8)
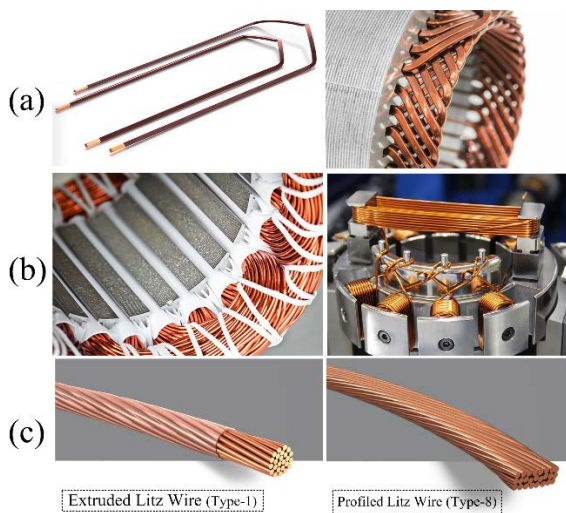
FIGURE 1. Different wire topologies. (a) Hairpin wires [22], (b) Single round conductor [23], (c) Litz wires [24], [25].

studies regarding the estimation AC loss in high frequency machines [4], [5], [6], [7], [8], [9], [10], [11]. Yet, most of these studies were considering limited frequency range or only one type of conductors, such as solid wires or stranded wires [12], [13], [14], [15], [16], [17], [18], [19], or rectangular wires [20], [21]. Therefore, in this paper, different magnet wire topologies and arrangements will be compared in a wider range of frequencies up to 2 kHz including rectangular hairpin wires, single round wires, and multi-strand or litz wires.

First, the enameled rectangular hairpin copper wires are a strong candidate for low and medium frequency electrical machines. With the highly automated manufacturing process of hairpin conductors, this technology is becoming more and more popular in different drive applications such as electric vehicles (EV) [26], [27], [28]. Compared to round or stranded conductors, rectangular wires have the advantage of high fill factor, which allows for lower losses at low frequencies.

A typical fill factor of such wires has a range between 60% - 70% [29]. However, at high frequencies, it may not be the best choice due to the excessive AC losses. Besides, there are extra procedures which are required for windings assembly such as pre-forming process, inserting process, and welding process [29], [30]. Fig. 1(a) shows an example of an electrical machine utilizing hairpin windings [22].

Secondly, the single round wire is frequently used in electrical machines due to its low-cost and high flexibility. This is why it is the ideal choice for different slot areas such as trapezoidal shape as shown in Fig. 1(b) [23]. However, one of the main disadvantages of such wire is that it has a limited copper fill factor, and therefore higher DC resistance and limited thermal conduction.

Thirdly, when the machine windings are carrying a high frequency current, the conductors are often divided into insulated multistrands, so that the current has a better distribution over the entire cross-section of each conductor. Also, for a further reduction of the eddy current losses, a transpositioning can be applied to the strands along the length of the wire, for example by twisting the strands. This conductor is known as Litz wire. With twisted insulated thin strands, litz wire has been considered as a practical solution to mitigate the AC losses in the conductors of the electrical machines, especially at high frequency operation. Besides electrical machines, litz wire has been a vital component in the design of many electromagnetic devices such as inductors [31], transformers [32]. The main problem of the multi-strand wires is the limited fill factor specially with a high number of twisted strands. A typical fill factor of the round extruded shapes of these wires has a range between 35% - 45% as reported in [29]. Additionally, to obtain the maximum possible fill factor, such wires can be designed in a profiled shapes such as rectangular litz wire as shown in Fig. 1(c) [24], [25]. Such shape is referred to as type-8 litz wire [33].

The main purpose of this paper is to take a step change in the design methodology and the magnet wire selection for electrical machines. This study is also targeting minimized conduction losses at high frequency by balancing between the AC and DC winding losses. Also, different topologies for conductors arrangement will be introduced in order to mitigate eddy current losses including proximity and skin effects. Moreover, finite element analysis (FEA) will be used to predict the AC copper losses at stranded level in which the current density and losses in each strand can be evaluated. Furthermore,, the performance of the four different coil designs will be measured and compared including stranded wire, litz wire and flat rectangular wire.

The paper is sub-divided as follows. In Section II, an analytical study is conducted for conductors at high frequency. Section III will be devoted to the baseline electrical machine and the behavior of current density at high frequency. In Section IV and Section V, different factors affecting the AC losses will be investigated. Also, different designs will be simulated using FEM in order to mitigate the AC high frequency losses. In Section VI, different prototypes

of winding coils will be implemented and experimented using either different magnet wires or different arrangements. In Section VII, a material tradeoff is made using multi-objective optimization. Finally, conclusions will be provided in Section VIII.

II. ANALYTICAL FORMULATION OF CONDUCTORS AT HIGH FREQUENCY

In order to calculate the power losses of a single conductor at high frequency, the distribution of current density should be evaluated. This can be carried out analytically using Maxwell's equations after assuming that the magnetic field has quasi-stationary conditions.

$$\begin{cases} \nabla \times \vec{E} = -\dfrac{\partial \vec{B}}{\partial t} \\ \nabla \times \vec{H} = \vec{J}_z \end{cases} \tag{1}$$

where E and B are the electric and magnetic fields, respectively. Also, H and J_z are the field intensity and current density vector along Z-axis, respectively. For linear material properties, it is known that $H = 1/\mu B$ where μ is the magnetic permeability of the medium. Using the second order differential equation of the current density vector along XY plane shown in Fig. 2, the equation of J_z is given as follows.

$$\frac{\partial J_z^2}{\partial x^2} + \frac{\partial J_z^2}{\partial y^2} = \beta^2 J_z \tag{2}$$

$$\beta = j\sigma\mu\omega \tag{3}$$

where ω is the angular frequency (rad/s), and σ the conductivity.

Since there is a big difference between the permeabilities of iron and air, the partial derivative along the X-axis can be neglected. Therefore, the equation of J_z can be simplified and solved as follows.

$$\frac{\partial J_z^2}{\partial y^2} = \beta^2 J_z \tag{4}$$

$$J_z(y) = C_1 e^{\beta y} + C_2 e^{-\beta y} \tag{5}$$

In case of a single conductor, the coefficients C_1, C_2 are obtained from the boundary conditions $H_x(0) = 0$, and $I = \vec{J}_z \cdot d\vec{S}$. Accordingly, J_z is given by:

$$J_z(y) = (\beta I/\omega) \cdot (cosh(\beta y)/sinh(\beta y)) \tag{6}$$

Using the expression of $J_z(y)$ in the equation of the Joule losses, the ratio the AC and the DC resistance $\varphi(\zeta)$ is obtained [34].

$$\varphi(\zeta) = \frac{R_{AC}}{R_{DC}} = \zeta \frac{sinh(2\zeta) + sin(2\zeta)}{cosh(2\zeta) + cos(2\zeta)} \tag{7}$$

where:

$$\zeta = h_c \sqrt{0.5\omega\mu\sigma} \tag{8}$$

$$\zeta = h_c/\delta \tag{9}$$

where h_c is the conductor height, and δ is identified as the skin depth. At high frequencies, when $\delta \leq 2h_c$ (i.e. $\zeta \geq 2$),

the ratio $\varphi(\zeta)$ has a linear variation with ζ. Accordingly, the effective cross section area is reduced and a higher current density is introduced near the conductor surface. This is the main reason for skin effect.

In case of multiple conductors, the following three boundary conditions are applied.

$$\begin{cases} H_x(0) = 0 \\ I = \vec{J}_z \cdot d\vec{S} \\ \oint \vec{H}_x \cdot d\vec{l} = I \cdot (k-1) \end{cases} \tag{10}$$

Accordingly, the current density in any conductor is obtained as follows.

$$J_{z,k} = \frac{\beta I}{\omega} \cdot \frac{kcosh(\beta y) - (k-1)cosh[\beta(y-h_c)]}{sinh(\beta h_c)} \tag{11}$$

where K is the conductor index as highlighted in Fig. 2. Using equation (11), the current density is modeled for 8 conductors at 1kHz as shown in Fig. 3. This will also be verified in the following section using FEM. Now, the AC power losses in each conductor can be calculated as follows.

$$P_{AC,k} = \frac{b_c L}{\sigma} \int_0^{h_c} |J_{z,k}|^2 \, dy \tag{12}$$

where b_c is the conductor width, L is the conductor axial length. Finally, the AC power losses is calculated as follows by considering uniform magnetic field distribution and an infinite permeability ferromagnetic material.

$$P_{AC,k} = \pi \frac{b_c L}{24} \omega^2 \sigma B_o^2 h_c^3 \tag{13}$$

where B_o is the peak value of the flux density.

From equation (13), it can be concluded that reducing the rectangle conductor height (which is raised to the power of 3) is one of the effective approaches to reduce the eddy current losses. Another way is to reduce the variation of the magnetic flux (B_o) across the conductors especially those near to the slot opening where high leakage flux exists. Therefore, leaving a space on top of the upper conductors is recommended in high frequency machines.
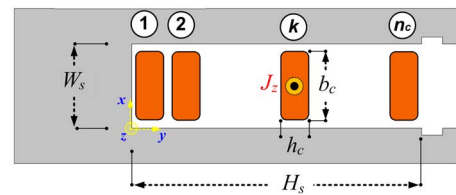

FIGURE 2. Winding model at strand level for a single slot.

III. BASELINE MACHINE AND SIMPLIFIED MODEL

A. BASELINE ELECTRICAL MACHINE

A three-phase synchronous reluctance machine is proposed as the baseline machine. Single-layer distributed windings are used for the 48-slot stator. Also, an 8-pole interior permanent magnet (IPM) rotor is used. This combination provides a high winding factor of 0.966. The motor rated speed
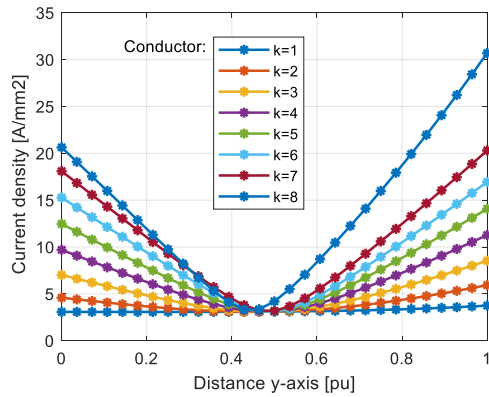
FIGURE 3. Current density analytical model results for 8 conductors at 1kHz.

FIGURE 5. Machine performance under sinusoidal current operation. (a) Rated input current. (b) No load back EMF. (c) Average torque. (d) Cogging torque.

is 15,000 rpm, which results in a 1-kHz base frequency. Further, the speed can be increased up to a maximum speed of 30,000 rpm, resulting in a 2-kHz fundamental frequency in the flux weakening region. The stator slots are designed with a parallel-sided shape to achieve a high fill factor for the flat conductors. The complete machine structure, winding layout, and FE model are shown in Fig. 4. Moreover, the machine performance is outlined in Fig. 5 under sinusoidal current operation. As can be seen, the cogging torque and the torque ripples are within the permissible limits (i.e. less than 5%). One of the major challenges of such design is the high AC losses due to the high magnetic field near the slot opening. That is why, in this paper, different winding topologies are investigated to mitigate the AC high frequency copper losses.

FIGURE 4. Reference three-phase IPM synchronous electrical machine: Machine configuration and FE model.

B. SIMPLIFIED REFERENCE MODEL

In order to simulate all these possibilities, a model simplification is necessary, because FEM of a complete electrical machine at stranded level is time consuming and sometimes not possible. In [35], a quarter of the machine is modelled including all parts; i.e. stator, rotor, and windings. The losses of this model are used as a baseline to assess any simplification of the machine. It was found that using a 1-slot model can result in an overestimation of the losses by 4.7%. Also, removing the rotor side can result in an underestimation of the losses by 1.3% with respect to the baseline model. Accordingly, the single slot model is used for evaluating the loss and optimization of strand position. Similarly, this study is
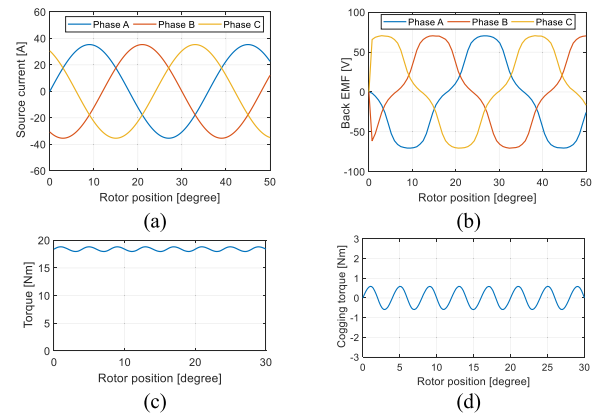
simplified by using two-slots model of a real electric machine as shown in Fig. 6(a). Due to space limitations in the paper, some figures show only one slot. However, the simulations are made for two slots.

C. CURRENT DENSITY AT HIGH FREQUENCY

In the conference version of this paper [1], the current density distribution at strand level is investigated for eight layers of a flat copper coil under the same current and frequency level. The results of this study are briefly repeated here for clarity. The current densities for the different layers are calculated at multiple points on a vertical line crossing all the conductors, and the magnitude and the phase angle values are shown in Fig. 6(b). It can be seen that there is a major difference between the current density distributions between the downstream and the upstream conductors. In the first conductor, the current density is almost uniform, and its variation as a function of position is nearly horizontal with a value lower than 4 A/mm2. However, as we get closer to the slot opening, the current density curve absolute value starts to become higher. For instance, in the upper layer, the current densities are very high at the upper and lower points with 33 A/mm2 and 22 A/mm2, respectively. Unlike the middle point in the same conductor, which has 4 A/mm2. Moreover, in each single layer, there is a 180° phase shift between the currents in the upper and lower points. Thus, both points are carrying the same current, but with the opposite directions.

In Fig. 7, the current density is investigated only for the upper layer at different frequencies. As can be seen, there is a big difference between low and high frequency operations. In DC operation, the maximum current density does not exceed 4 A/mm2. However, at 2 kHz, its value can exceed 60 A/mm2, i.e. 15 times higher. Thereby, it can be said that the upper layer is the weak part in the coil design.

This crucial non-uniform current distribution – caused by the skin and proximity effects – will result in the increase of the apparent resistance of the coil. Accordingly, the AC losses will remarkably increase at high frequency operation.

Case (I): Flat conductor
"Reference case"

Case (II): 10 strands

Case (III): 45 strands
8 layers x 1 conductor

Case (IV): 45 strands
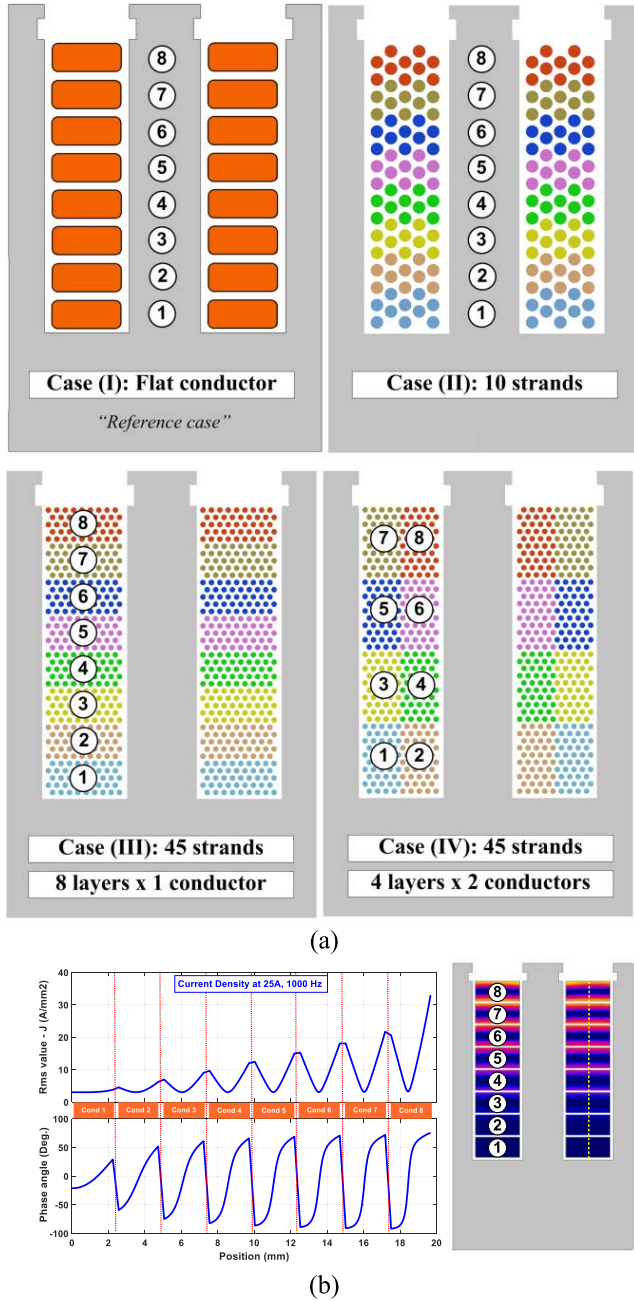4 layers x 2 conductors

(a)

(b)

FIGURE 6. (a) Investigated case studies using simplified model. (b) Current density distribution at strand level for different layers in the reference case study.

That is why, in this paper, different design possibilities will be investigated in order to mitigate the AC high frequency losses.

IV. WINDING DESIGN AND AC COPPER LOSS

If you are using Word, use either the Microsoft Equation There are many factors that can affect the total winding losses in the electrical machines such as conductor type (i.e. solid or stranded), and the location of each conductor inside the slot. In this section, the following factors are investigated.
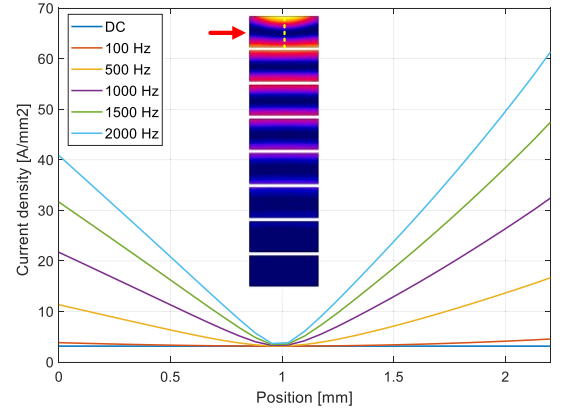
FIGURE 7. Current density distribution for the upper layer at different frequencies.

- Number of conductors
- Fill factor
- Number of strands
- Conductor arrangement
- Strand positioning

The losses in the reference 2-slot motorette can be divided into two main components. The first one is due to the net copper losses (P_{Cu}), which is mainly the sum of DC and AC copper losses, and the second one is due to the iron losses in the machine core (P_{ir}). The equation is expresses as follows.

$$P_{Total} = P_{Cu} + P_{ir} \tag{14}$$

$$P_{Total} = P_{DC} + P_{AC} + P_{ir} \tag{15}$$

A. NUMBER OF CONDUCTORS

For the same slot area, different numbers of conductors are simulated as shown in Fig. 8. For a fair comparison, as the number of conductors increases, the simulation current is reduced by the same percentage so that the total ampere turns (ATs) of each slot will be identical between the cases. For instance, in the example shown in Fig. 8, the number of conductors used are 2,4,8, and 10, so the simulation currents are 100A, 50A, 25A, and 20A, respectively. Under the same frequency of 1 kHz, it can be observed that the maximum current density has excessive value when using the 2 or 4 conductor per slot. However, these values can be remarkably reduced as the number of conductors increases to 8 or 10. For instance, it has only 51% of its value when using 10 conductors instead of 2 conductors.

In Fig. 9 (a), both copper and core losses are calculated as a function of frequency for the different number of conductors under the same ATs value. As can be seen, the effect of number of conductors on the core losses is quite limited. However, copper losses can be effectively attenuated at high frequency by using higher number of conductors. For instance, in Fig. 9 (b), the total power losses at 1 kHz can be reduce by nearly 60% when using 8 conductors instead of 4 conductors. However, with the higher number of conductors, the manufacturing time and cost will increase specially
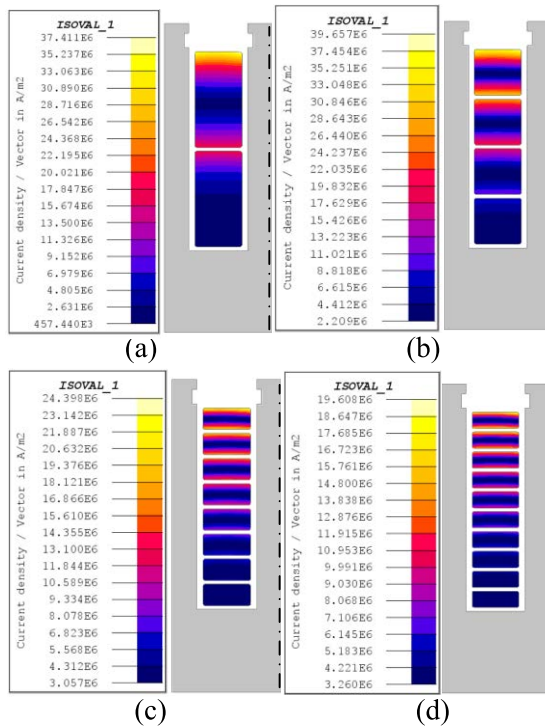
FIGURE 8. Current density distribution for different numbers of conductors under the same ampere turns and a frequency of 1 kHz. (a) 2 conductors, (b) 4 conductors, (c) 8 conductors, (d) 10 conductors.
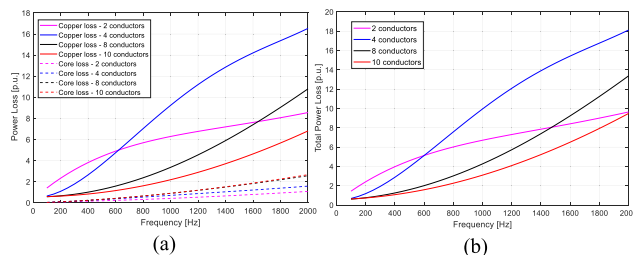

FIGURE 9. Power losses for different number of conductors at different frequencies under the same ampere turns. (a) Loss components: net copper loss, iron loss. (b) Total power loss.

if it is associated with welding. That is why trade-off should be made in order to select the best feasible option.

Interestingly, at very high frequencies (e.g. 2 kHz), it is noticed that the 2-conductors model has lower losses than the 4-conductors or 8-conductors models. The main reason is that proximity effect is increasing faster than skin effect at this frequency zone.

B. FILL FACTOR

For the same number of conductors, the coil simulation is conducted at different fill factors using different layer heights as shown in Fig. 10. The fill factor could be reduced due to the need for thicker insulation which more evenly affects the copper distribution in the slot. Three different designs are presented having a fill factor of 90%, 60%, 40%. The corresponding conductor areas are A_1, A_2, and A_3, respectively. First, under dc excitation, as the height deceases, the

current density dramatically increases from 3.16 A/mm^2(A_1) to 5.26 A/mm^2(A_3). However, under high frequency excitation of 1 kHz as shown in Fig. 10, the maximum current density unexpectedly has reduced despite the cross-sectional area is getting lower ($A_{1\rightarrow3}$). Additionally, the total losses of each case are calculated at different frequencies as shown in Fig. 11. As can be seen, at frequencies up to 250 Hz, the coil with the highest fill factor (A_1) shows the lowest losses. At higher frequencies between 250 Hz and 470 Hz, relatively lower losses are realized by the second design (A_2). Above 470 Hz, the coil with lowest height (A_3) has the best performance. Therefore, it can be concluded that using of larger size conductors does not necessarily mean that the losses will be lower.
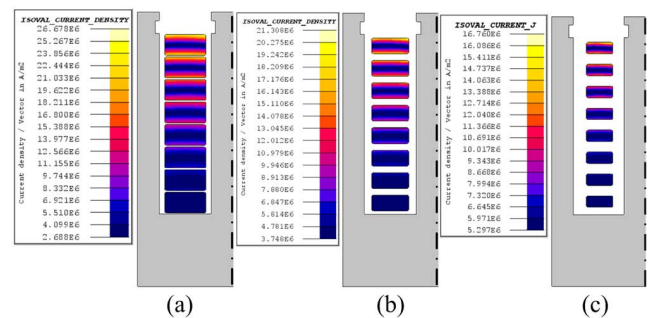

FIGURE 10. Current density distribution under different fill factor for the same number of conductors. (a) 90% fill factor. (b) 60% fill factor. (c) 40% fill factor.
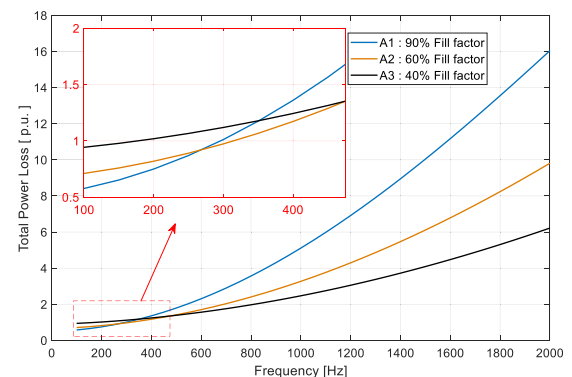

FIGURE 11. Total power losses for different fill factors at different frequencies.

C. NUMBER OF STRANDS

As mentioned in the previous section, the solid conductors have the advantage of high fill factor. However, at high frequency, this can be a major problem due to the high skin and proximity effects. Alternatively, the stranded wires can be a better option to avoid excessive high frequency losses. Two different multi-strand coils are simulated. The first coil has low number of strands (10 thick strands) and the second one has high number of strands (45 thinner strands). The current densities of both cases are compared with the solid single flat copper coil as shown in Fig. 12 (a-c). At 1 kHz,
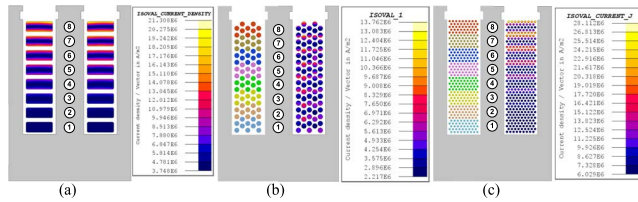
FIGURE 12. Current density distribution for different number of strands at 1 kHz: (a) Single solid conductor, (b) 10 strands, (c) 45 strands.
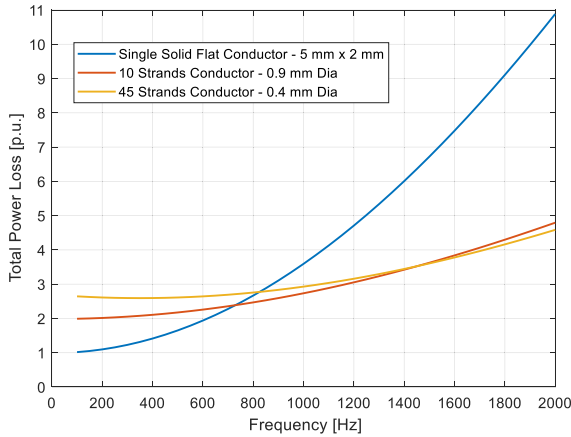

FIGURE 13. Total power losses at different frequencies, for three cases with different numbers of strands as shown in Fig. 12.

the 10-strands wire has reduced remarkably the maximum current density compared to the solid flat coil by about 35.7 % i.e. from 21.3 A/mm2 to 13.7 A/mm2. When the number of strands increases further to 45 thinner strands, it can be seen that the current density increases in the upper conductor up to 28.1 A/mm2. Thereby, it can be concluded that at a certain frequency level, increasing the number of strands can be effective for reducing AC losses up to a certain limit. The power losses of the three cases are compared at different frequencies in Fig. 13. Obviously, the single solid conductor has lowest losses up to 750 Hz. However, above this frequency, the 10-stands wire will provide lower losses. Nevertheless, at very high frequencies (above 1500 Hz), the 45-strand conductor shows a relatively better performance compared to the 10-strands one. The results are shown in P.U. So, the reference 1 P.U. is equal to the total power loss in the flat copper coil at 100 Hz.

D. CONDUCTOR ARRANGEMENT

Stranded wires have various arrangements inside the slots of electrical machines. This type of conductors can be randomly placed inside the slot or it can be arranged in a regular shape. For a more precise comparison, the stranded wires are arranged in two regular shapes using the same number of conductors and strands. In the first case, the conductors are stacked vertically in one column with 8-horizontal-layers and one 45-strands conductor in each layer as shown in Fig. 14(a). In the second case, the conductors are arranged vertically in 4 layers with two 45-strands conductors in each layer as

shown in Fig. 14(b). In terms of current density, it can be noticed that using the vertical arrangement leads to increasing the maximum current density by more than 75% at 1 kHz.

The copper losses are also compared in Fig. 15 within the main frequency range (100 Hz – 2 kHz) and higher frequency up to 10 kHz. Evidently, reducing the number of layers increases the coil copper loss dramatically within the main frequency range. Thereby, it can be concluded that placing the conductors horizontally in one column on top of each is the optimal arrangement for an electrical machine. It also worth mentioning that the vertical arrangement shows only lower copper losses at very high frequencies starting from 5 kHz. So, such an arrangement may be suitable for other types of applications such as high frequency wireless power transfer.
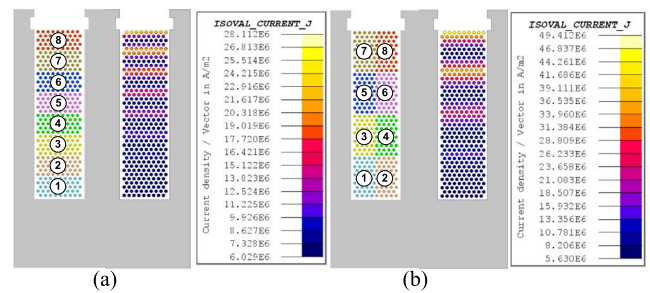

FIGURE 14. Current density distribution for different arrangements of conductors at 1 kHz. (a) Horizontally-laid (8 layers × 1 conductor). (b) Vertically-laid (4 layers × 2 conductors).
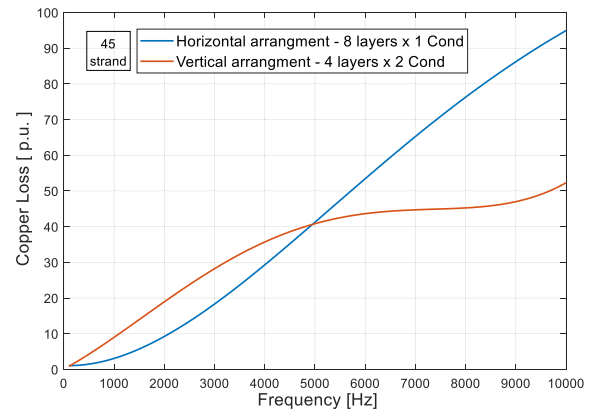

FIGURE 15. Net copper losses at different frequencies for two different arrangements as shown in Fig. 14.

E. STRAND POSITIONING

In multi-strand windings, it is hard to control the position of each strand inside the coil. To demonstrate the effect of the uncontrolled positioning of the strands that would happen in practice, two designs for a 10-strands coil are compared with two different strand positionings as shown in Fig. 16. In the first case, the strands position is ideal and each strand has a fixed location. However, in the second case, using a special pattern, the strands are transposed in such a way that each strand has a different position in each layer. Thus, the proximity and eddy current losses can be remarkably reduced.
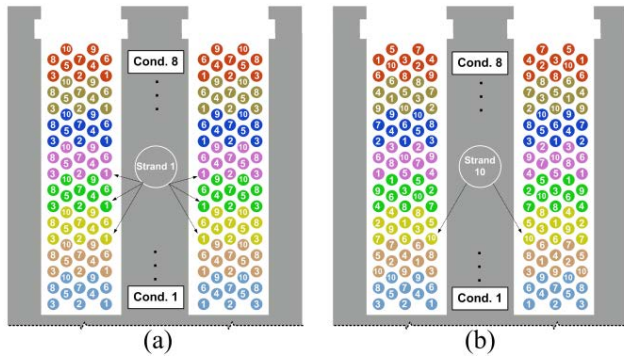
FIGURE 16. Different allocation of strands for the same 10-strand conductor. (a) Non-transposed strands. (b) Transposed strands.
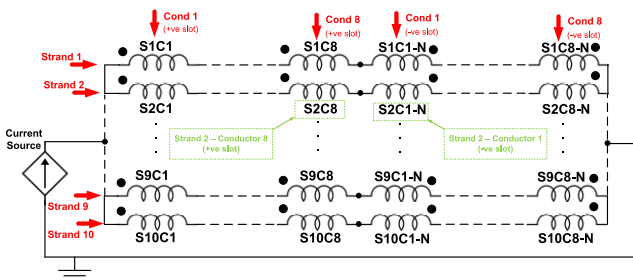

FIGURE 17. The electrical circuit for a 10-strand coil with 8 turns.
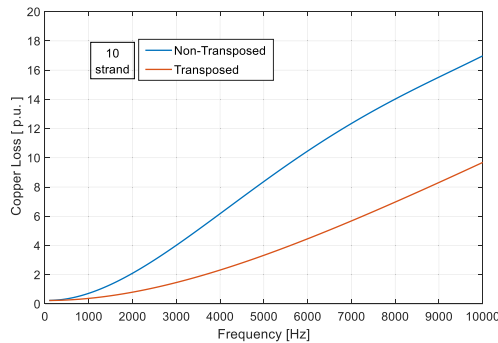

**FIGURE 18.** Effect of strands transposition on the net copper losses at different frequencies.

The position of each strand is indicated by the small white number inside each conductor.

The same electrical circuit is used to simulated both of the 10-strands coils as shown in Fig. 17. It can be noticed that the circuit has 10 parallel branches representing the 10 strands. In each branch there are 8 conductors for the positive slot in series with additional 8 conductors for the negative slot.

The copper losses are calculated for both of the non-transposed and transposed strands in Fig. 18 for a wide range of frequencies between 100 Hz to 10 kHz, As can be seen, the transposed-strand conductor has remarkably lower losses compared to the one with fixed strand positions. The loss difference can be clearly seen at higher frequencies rather than lower frequencies. Furthermore, the copper losses are compared at strands level and inspected for each individual
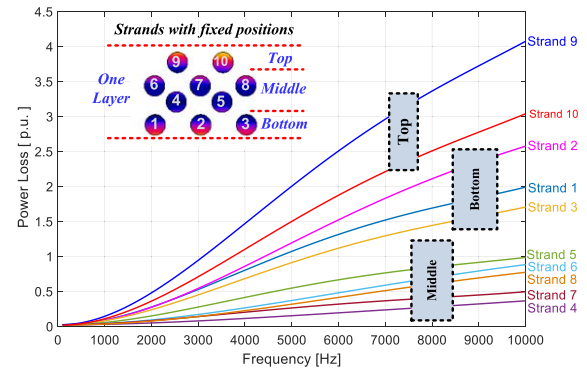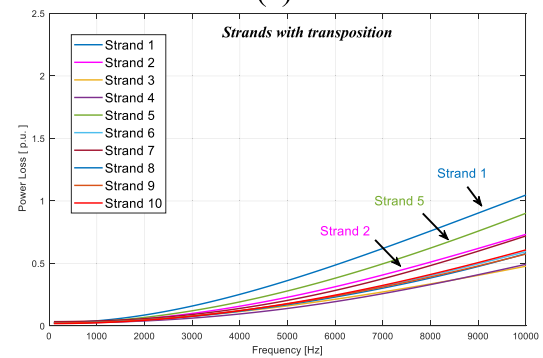
FIGURE 19. Copper losses at strands level. (a) Non-transposed strands. (b) Transposed strands.

strand as shown in Fig. 19. When the strands has a fixed position [Fig. 19(a)], the losses are high at the top and bottom strands of each layer, which are 50% of the total number of strands. However, with transposition [Fig. 19(b)], it is noticed that 90% of the total number of strands have remarkably low copper losses.

V. CORE DESIGN AND AC COPPER LOSS
The core design can also have an impact on the AC copper losses. In this section, the following factors are investigated.

- Effect of adjacent slots
- Slot opening shape
- Rotor presence and airgap length
- Core material

All these case studies are simulated and compared in the following subsections.

A. EFFECT OF ADJACENT SLOTS
In the previous sections, a single coil is simulated along with a single E-core without any consideration of current in the side slots. This section investigates if there is any possible impact of the side slots on the copper and core losses. Accordingly, the core is placed between two similar cores and the side coils are carrying the same current. In Fig. 20(a), the side slots have a current direction similar to the investigated coil, that is why there are no flux lines in the side teeth of the investigated coil. As a result, the associated core losses are much lower
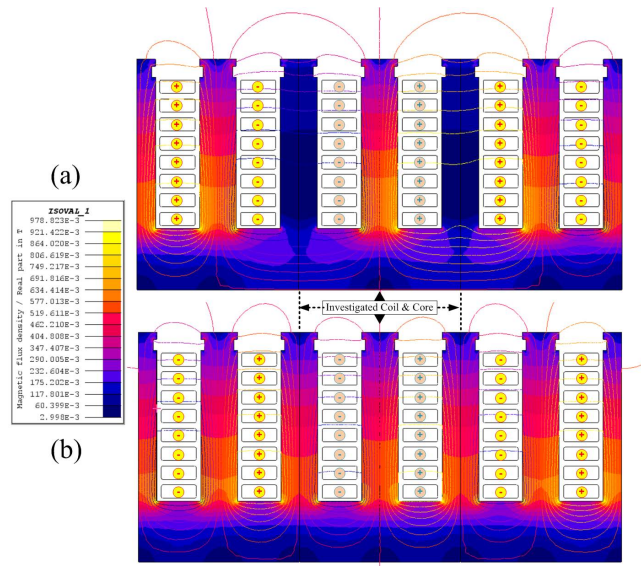
FIGURE 20. Effect of current in the side slots on the magnetic flux density of the core at 1 kHz. (a) Same current direction. (b) Opposite current direction.
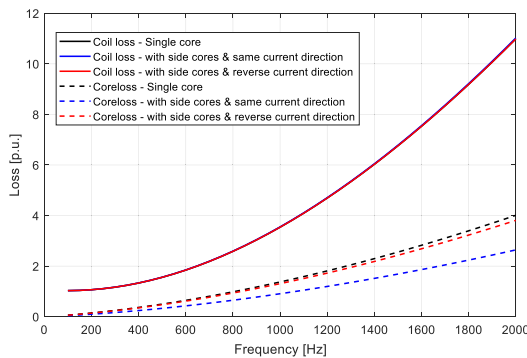

FIGURE 21. Effect of side cores on the net copper losses and the core losses.

FIGURE 22. Effect of slot opening shape on the leakage flux and the magnetic flux density in the core at 1 kHz. (a) Open slot. (b) Semi-closed slot. (c) Closed slot.

FIGURE 23. Effect of slot opening shape on the net copper losses at different frequencies.

as noticed in Fig. 21. On the other hand, when the side slots have a reversed current direction as shown in Fig. 20(b), the flux lines flow normally through the side teeth. Thus, the core losses are closer to the single core case. As for the net copper loss, the conduction loss seems to be unaffected by proximity of the side coils as seen in Fig. 21.

B. SLOT OPENING SHAPE

The slot opening dimensions have a major impact on the leakage flux, which in turn can affect the AC copper losses. In this section, three common designs for the slot opening are simulated in Fig. 22, which are open, semi-closed, and closed slots. Also, the copper losses are calculated for each slot shape as shown in Fig. 23. It is observed that the copper losses have almost the same profile up to 800 Hz for all the cases. However, above this frequency, the closed slot design seems to have slightly lower copper losses. This is because the coil upper layer is exposed to lower leakage flux. Additionally, in terms of the saturation state of the teeth of the closed slot, the tooth flux density is already increased to a level where the
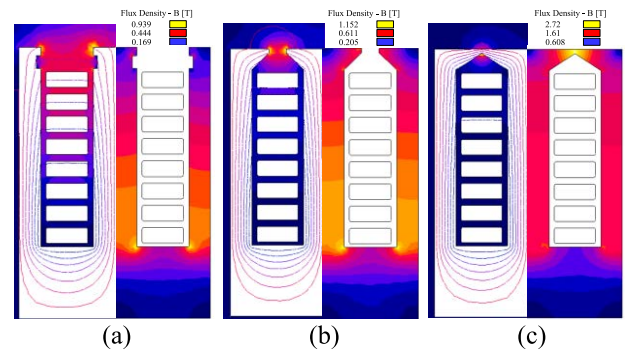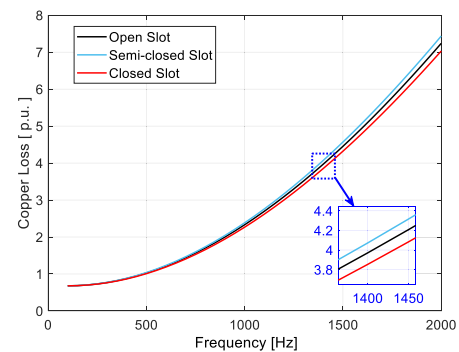
permeability starts to drop. This reduces total leakage flux as well. On the other hand, the semi-closed slot causes the highest copper losses, because the coil is exposed to relatively higher leakage flux as shown in Fig. 22.

C. PASSIVE ROTOR PRESENCE AND AIRGAP LENGTH

In this section, the effect of the rotor presence is investigated using variable airgap length as shown in Fig. 24(a, b). As can be seen, when the rotor is fully aligned with the stator teeth, the magnetic flux density increases remarkably, especially at the teeth when comparing to the core without a rotor. So, the permeability in the saturated parts of the teeth starts to drop. This reduces total leakage flux. Accordingly, the copper losses will be lower when the rotor side is in front of the slot opening as shown in Fig. 25. It is concluded that the AC losses are significantly impacted by the saturation state of the iron (especially the teeth), which in this case has been realized by reducing the air gap length. In a real machines, the saturation state of the iron is a result of the combined rotor and stator magnetic field. This total effect should therefore be taken into account in the AC loss calculation. It also obvious that the lower the airgap length, the lower the copper losses would be. Yet, this is not a general case since the rotor can contain PM field that is pushing the d-axis armature reaction field back to the stator core causing more slot leakage flux and strong circulation current issue.
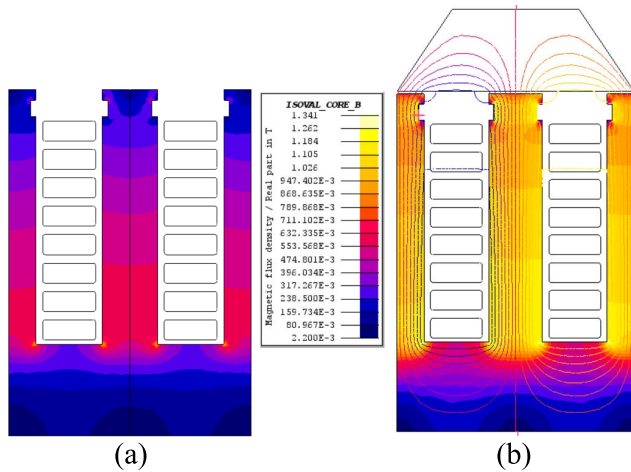
FIGURE 24. Effect of rotor presence on the magnetic flux density in the core at 1 kHz. (a) Without rotor side. (b) With rotor side.
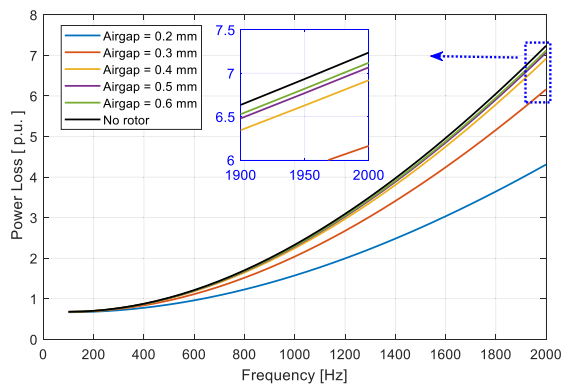

FIGURE 25. Effect of rotor presence and airgap length on the copper losses at different frequencies.

D. CORE MATERIAL

The simulation of the single core is conducted for different materials to investigate their impact on the AC copper losses. Also, in order to allow maximum possible flux density within each material, a rotor segment is added to each core as shown previously in Fig. 24(b). The B-H curves of these materials are shown in Fig. 26. These materials have different saturation levels starting from above 2 T for the cobalt iron (HIPERCO50) down to lower than 0.5 T for the soft ferrites. Additionally, the corresponding copper losses are calculated at Fig. 27. As can be seen, the losses in the air core coil seem to be quite limited and the losses curve is nearly horizontal, i.e. slightly affected by the higher frequency excitation. Using soft magnetic materials with a saturation level lower than 1.5 T will result in a limited increase in the AC losses, specially at high frequency. Moreover, when the core magnetic material has a saturation level above 1.5 T, the AC copper losses increase exponentially with frequency.

VI. PROTOTYPING AND EXPERIMENTATION

In order to verify the simulation results, a motorette (a fraction of the baseline machine) in the form of E-core is manufactured with 2 parallel-sided slots and open slot design
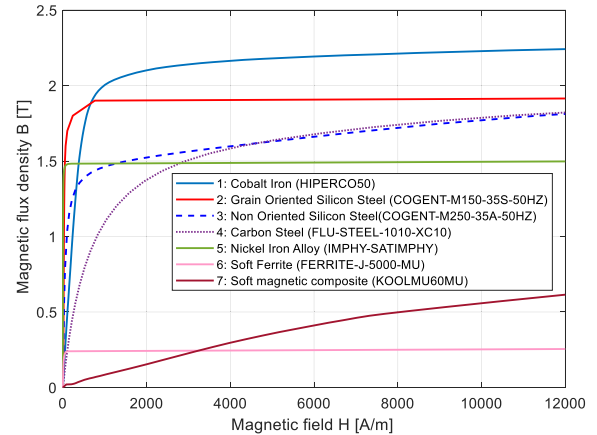

FIGURE 26. B-H curves of for the investigated different core materials.
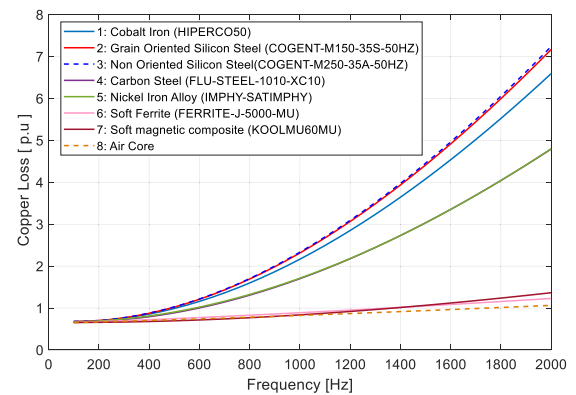

FIGURE 27. Effect of different core materials on the net copper losses.

as shown in Fig. 28(a). For a fair comparison, four identical E-cores from Fe-Si with four different winding samples are prototyped. All the measurements are made at a fixed temperature of 25°C. A specially designed cooling jacket is also used with a water chiller to maintain the temperature at a constant level [see Appendix A]. Additionally, the test is performed at each frequency level for less than 2 seconds, so that the temperature of the coil samples remains unaffected for the considered current level.

The first sample is the flat copper coil with 8 turns and a rectangular cross sectional area of 5 mm × 2 mm as shown in Fig. 28(a). With the relatively high tensile strength of this thick copper wire, a special bending machine is used to make it with a perfect fit within the slot area and with a minimum end turn overhang. In the second sample, a parallel strand wire is used to build a coil with the same number of turns. Each turn has 10 insulated strands with 0.9 mm diameter as shown in Fig. 28(b).

In the third and fourth samples in Fig. 28(c), a custom-made type-8 litz wire is manufactured with a rectangular shape. Each coil has also 8 turns, and each turn includes 45 insulated strands with 0.4 mm diameter. An outer thin film is used to compress the strands together with an outer dimensions equal to the flat copper coil, i.e. 5 mm × 2 mm. The main difference between both samples is the arrangement
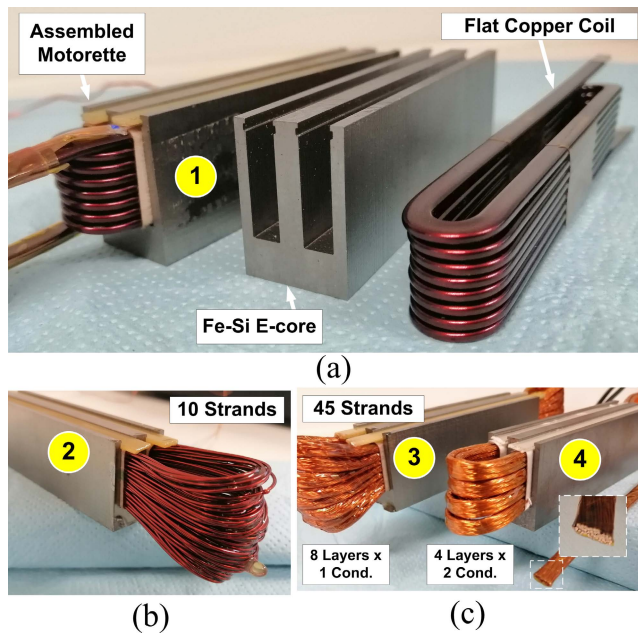
FIGURE 28. Assembled winding prototypes. (a) Flat rectangle. (b) 10 strands. (c) 45 strands with two different arrangements.
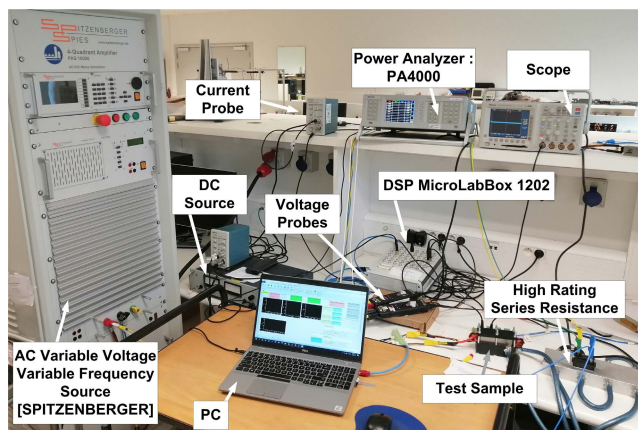

FIGURE 29. Test setup.

of the conductors inside the slot as previously showcased in Fig 14. In the third sample, the conductors are arranged horizontally in one column with 8 layers, so that each layer has only one conductor. However, in the fourth sample, the conductors are arranged vertically in two columns with 4 layers, so that each layer has two conductors.

The four samples are tested using the test platform shown in Fig. 29. It consists mainly out of a DC and AC voltage sources, voltage and current sensors, and data acquisition (DAQ) system. The DC source is used for the DC losses measurements. Also, a linear amplifier of 40 A and 270 V (Spitzenberger) is used as an AC variable voltage variable frequency input source for the AC loss measurements. Additionally, voltage and current probes are used to measure the voltage and the current of the test sample. Moreover, a dSpace MicroLabBox 1202 is used as a real time interface and for DAQ. There is also a PA4000 (Tektronix) power analyzer
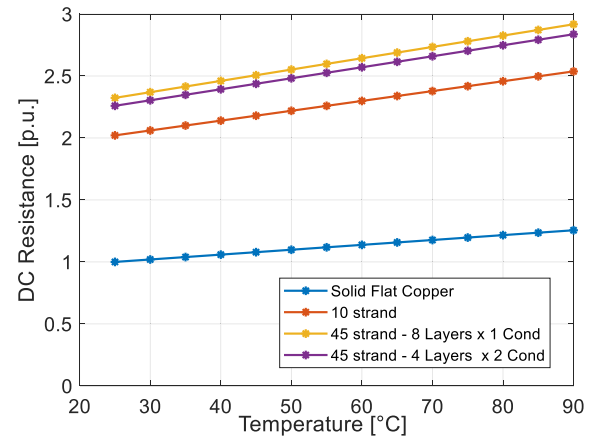

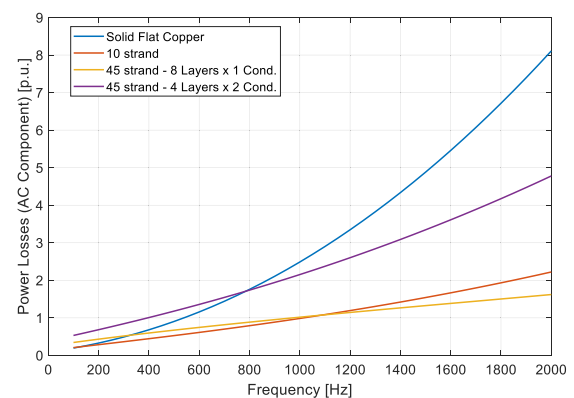**FIGURE 30.** The measured DC resistance of the different coils as a function of temperature.

FIGURE 31. The measured AC component of the net copper loss at different frequencies.

used to measure the AC and DC losses. A scope (Tektronix TDS3054 4-Channel) is used to monitor the waveforms. Finally, in order to perform the loss measurements at high sinusoidal currents, the test sample is connected in series with a water-cooled power resistor. This zero-inductance resistance is useful to maintain sinusoidal current waveforms at high frequencies.

As for the DC test, the DC losses of the different samples are measured at different temperatures and the DC resistance of each coil is calculated as a function of temperature as shown in Fig. 30. As can be seen, the flat copper coil has remarkably lower DC resistance because of the higher fill factor along with the shorter end turns. On the other hand, all the stranded types have higher DC losses due to the relatively lower fill factor. Among the three stranded types, the 10-strand coil has lowest losses due to the slightly high fill factor with respect to the 45-strand types. It also noticed that the DC resistances of the two 45-strand coils are almost equal. The slight difference between them is mainly due to the shorter end turns in the case of vertical arrangement resulting in a slightly lower DC resistance.

The AC measurements are also conducted for all the coils at different frequencies up to 2 kHz under the same current
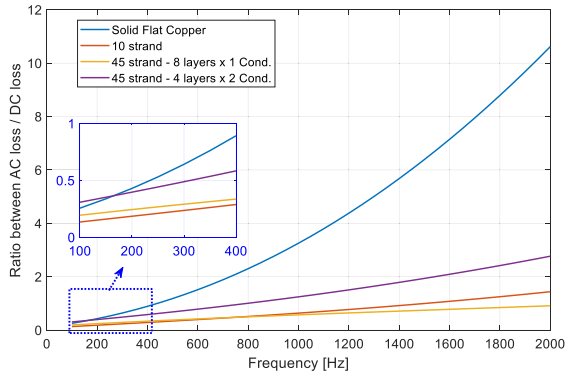
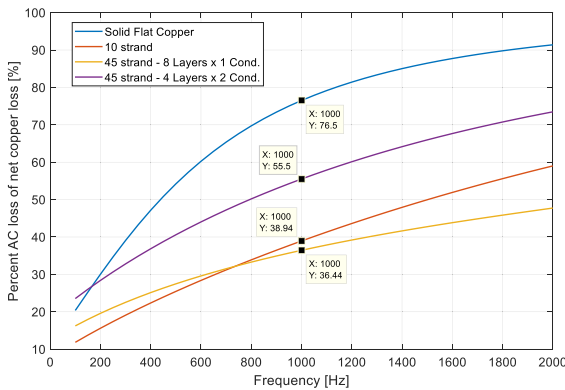**FIGURE 32.** The ratio between the AC to DC losses at different frequencies.

FIGURE 33. The percentage of AC loss from the net copper loss at different frequencies.

FIGURE 34. The total measured power loss components for the different coils at different frequencies.

FIGURE 35. The net copper losses: comparison between simulation and measurement losses at different frequencies.

level. The winding power loss is separated by subtracting the iron loss from the total measured losses. An accurate iron loss model was used for this aim. The results of all the figures are shown in P.U. So, the reference 1 P.U. is equal to the total measured power loss in the flat copper coil at 100 Hz, as it will be shown later in Fig. 36. In order to calculate the AC copper loss component for each coil, the computed iron losses and the measured DC copper losses are subtracted from the total measured losses. The AC component of the copper losses (P_{ac}) is compared for the different samples as shown in Fig. 31. It can be seen that the 10 strands coil has the lowest AC loss up to 1.1 kHz. Above this frequency, using a 45-strands coil with a horizontal arrangement will provide a lower AC loss. Moreover, it is observed that the flat solid coil has excessive AC losses above 800 Hz. Also, the ratio between the AC to DC losses is computed at different frequencies as shown in Fig. 32. Additionally, the AC loss component is calculated as a percentage of the net copper losses (P_{Cu}) as illustrated in Fig. 33. It is clear that the percent of AC losses is very high for the solid flat coil along almost the entire frequency range. For instance, at 1 kHz, the flat solid coil has 76.5% of its net copper losses only for the AC loss component. At the same frequency, this percent is 55.5%, 38.9%, and 36.44% for the 45-strand-vertical coil, 10-strand coil, and 45-strand-horizontal coil, respectively.
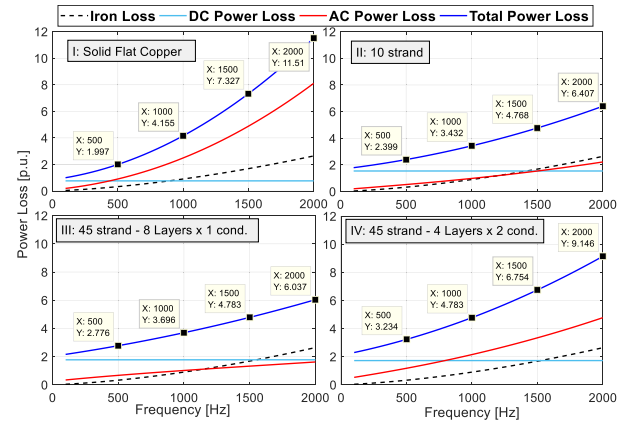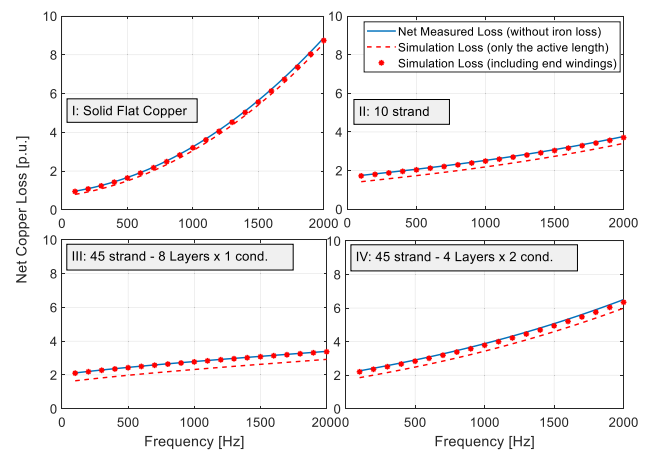
The total power loss is also measured for each case as shown in Fig. 34, including its three components, i.e. iron loss, DC loss, and AC loss. In the solid flat coil, the AC loss (i.e. the red line) crosses the DC loss (i.e. the aqua line) at a low frequency of 400 Hz. In the 10-strand coil, the AC loss stays under the DC loss up to a higher frequency of 1500 Hz. In the 45-strand-horizontal coil, the AC loss is completely under the DC loss for the specified frequency range. On the other hand, the AC loss of the vertical arrangement crosses the DC loss earlier at 750 Hz, despite they both have nearly the same DC losses. In terms of core losses, all the four samples have almost the same exact level, since the tests are conducted using the same core under the same ampere turns.

Finally, the net measured copper losses are compared with the simulated results as shown in Fig.35. Very good agreement is achieved between both results after accounting for the end turn losses. Also, the total power losses are compared for the different coils in Fig. 36. It can be concluded that using flat solid coil will provide the lowest total losses at low frequency up to 700 Hz. Above 700 Hz, a 10-strands wire will have a remarkably lower losses compared to the solid
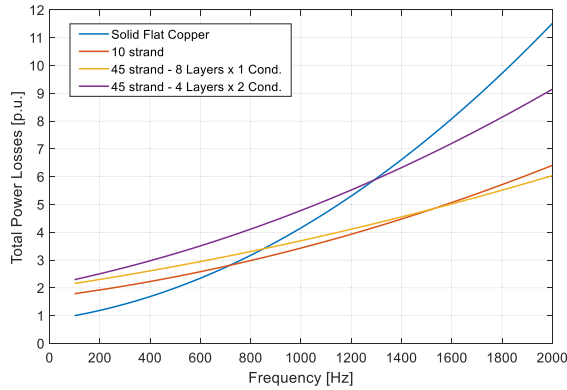
FIGURE 36. Comparison between the measured total power loss for the different coils at different frequencies.

conductor. Above 1500 Hz, a 45-strand wire with horizontal arrangement can even have a better performance compared to the 10-strand coil. Moreover, along the specified frequency range, the 45-strand-vertical coil has the worst case scenario of losses. The only exception is frequencies above 1300 Hz, at which this coil overcome only the flat solid coil. However, it is expected that this coil will provide a better performance at frequencies above 5 kHz, as verified in the simulation results.

To sum up, a comparison between the different coils is summarized in Table 2 along with the specifications of each case. It can be deduced that flat solid rectangular conductor (Coil I) can have a high fill factor. However, a low frequency operation is a must to guarantee a good performance. Also, higher cost and longer time are required due to the hard conductor formation, which may be associated with welding in case of hairpins. On the other hand, an alternative option of thick parallel multi strands (Coil II) can have a relatively lower fill factor and longer end turns. However, a better performance can be realized at medium frequency ranges. Besides, there is no much time or cost are spent on the conductors bending, due to the high flexibility. Finally, using high number of strands combined with strands transposition can result in a lower fill factor as in coil III. However, the coil performance can be better at high frequencies starting from 1.5 kHz. Moreover, if the same conductors are arranged vertically, the losses can be even reduced starting from 5 kHz as the case of coil IV. Additionally, the bending will be relatively easier, which results in a shorter end turns and lower coil weight.

VII. MULTI-OBJECTIVE OPTIMIZATION

Apart from electric losses, weight and cost play an important role in the selection of the winding topology. That is why using lightweight conducting material is highly important for certain applications. Therefore, in this section, aluminum is used as an alternative to copper. A parametrized model is built with variable strand cross section areas and variable materials for each strand using the reference coil with 8 flat conductors. All input variables are highlighted in Fig.37 and listed in Table 3. Targeting minimum loss, weight, and cost,

TABLE 2. Comparison between different winding topologies.

|	Coil I	Coil II	Coil III	Coil IV
Conductor type	Flat Solid	Thick Strands	Thin Strands Horizon.-laid	Thin Strands Vertically-laid
Shape	Rectangular shape	Round parallel strands	Type-8 Litz	Type-8 Litz
Number of strands	1	10	45	45
Strand Gauge	7 AWG	19 AWG	26 AWG	26 AWG
Conductors arrangement	8 layers x 1 conductor	8 layers x 1 conductor	8 layers x 1 conductor	4 layers x 2 conductor
Slot Opening	Open @ radial-insert (Semi) Closed @ axial-insert	Open / Semi-closed	Open / Semi-closed	Open / Semi-closed
Slot Shape	Parallel slots	Custom	Parallel slots @ Type-8 Custom @ Type-1	Parallel slots @ Type-8 Custom @ Type-1
Coil Weight	172.8 gm	171.3 gm	162.9 gm	146.8 gm
Fill factor	72.7 %	46.2 %	41.1 %	41.1 %
DC losses	Lowest (1 p.u.)	High (2.02 p.u.)	Highest (2.32 p.u.)	High (2.26 p.u.)
AC losses	Highest (76.5% @1kHz)	Low (38.9% @1kHz)	Lowest (36.4% @1kHz)	High (55.5% @1kHz)
Preferable frequency range	DC − 700 Hz	700 Hz − 1500 Hz	1.5 kHz - 5 kHz	>= 5 kHz
Possible application	Dc machines, Low frequency machines : e.g. EV, aircrafts, naval machines at 400 Hz [36].	High speed (HS) electrical machines [37].	Super HS machines [38]: Handpiece dental drills @ 4 kHz	High frequency wireless power transfer[39]. EV fast charging units.
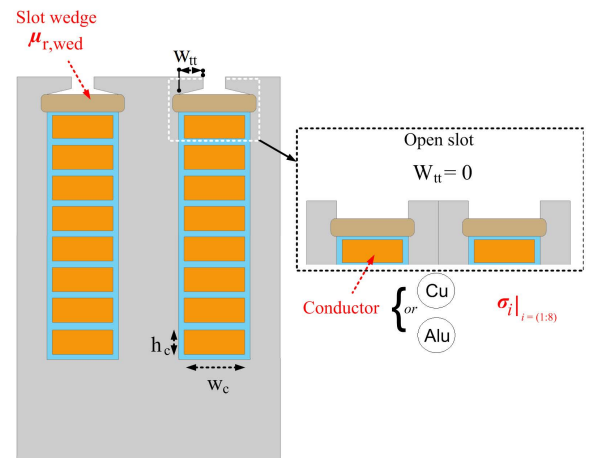
FIGURE 37. Parametric model at strand level.

10,000 designs are investigated in this optimization model. The weight and cost are estimated for the baseline 48-slot machine as shown in Fig. 38. It is noticed that the full copper coil cases have low losses. However, the weight and cost are very high. On the other hand, full aluminum coil cases have relatively higher losses, but the weight and cost are remarkably lower. It is also noted that using a combination between copper and aluminum in each slot results in minimizing all of
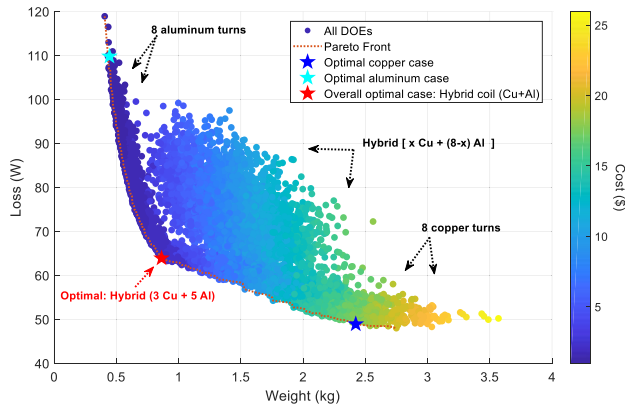
FIGURE 38. Multi-objective optimization for the reference coil case with 8 flat conductors using variable strand material.
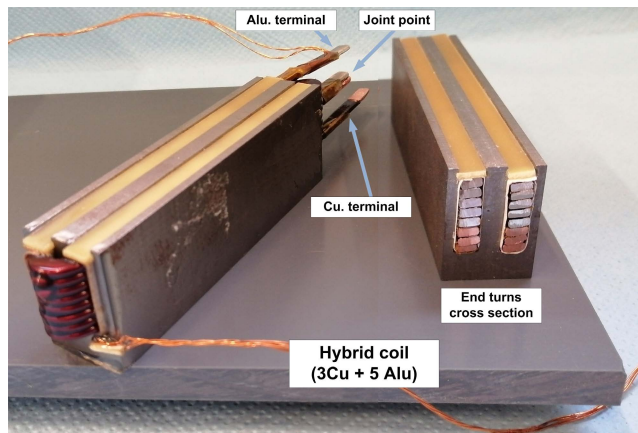

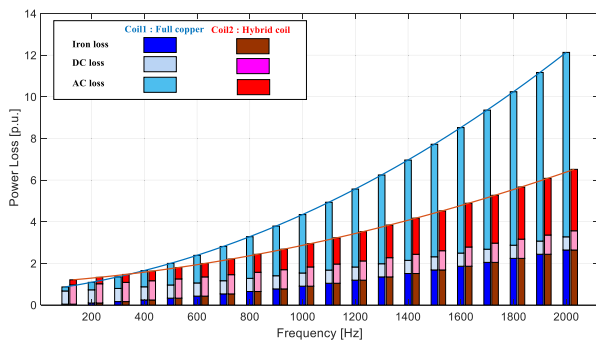**FIGURE 39.** Prototyping of flat rectangle coil with hybrid material conductors.

FIGURE 40. The measured total power loss for the hybrid coil compared to the full copper one at different frequencies.

TABLE 3. Variables of the multi-objective optimization.

Input Parameters	
Conductor height	h_c
Conductor width	w_c
Tooth tip width	w_{tt}
Resistivity of each turn (Cu or Al)	$\sigma_i \mid_{i=1 \to 8}$
Permeability of the slot wedge	$\mu_{r,wed}$
Output Function and Objectives	
$minimize \begin{cases} \textbf{Loss (W)} \\ \textbf{Weight } (\textbf{kg}) \\ \textbf{Cost } (\$) \end{cases}$	

copper coil as shown in Fig. 40. As can be seen, the AC losses are remarkably reduced at the high frequency domain.

VIII. CONCLUSION

In this paper, the AC losses for different wire topologies are inspected at stranded level. The main contribution of this study is that more parameters are investigated and validated for the same slot topology than in any other previous work, offering a quick overview to readers of the expected conductor losses for given winding details. Using finite element analysis, the eddy current losses and current density distribution in the machine conductors are simulated for different conductor shapes or arrangements including rectangular, stranded, and litz wires. Moreover, for a better mitigation of AC losses, different factors that may affect the winding losses are studied, such as number of layers, fill factor, number of strands, conductor arrangement, strands transposition, slot opening shape, rotor presence, and core material. Furthermore, four winding samples are prototyped using either different magnet wires or different arrangements. The measured total power losses are decomposed into three main components, which are DC loss, AC loss, and iron loss. The AC components for all the topologies are compared at a wide frequency range.

The main conclusions are summarized in the following points. Firstly, in terms of winding design:

- With higher number of layers, the AC losses decrease by nearly 60%. However, the fill factor decreases and consequently the DC losses increase. Besides, a higher manufacturing cost will be required. That is why a tradeoff is necessary to select an optimal number of conductors based on the application frequency.
- Proper arrangement of the conductors inside the slot is very crucial for limiting the AC losses. For instance, when the 45-strand conductor is laid in 4 layers with 2 conductors per layer instead of 8 layers with 1 conductor per layer, the AC losses have almost doubled despite using the same exact wire and the same number of turns under the same operating conditions.

Secondly, in terms of operating frequency recommendations for the investigated cases:

the losses, weight, and cost. In this particular case, it is found that using 3 turns of copper with 5 turns of aluminum results in nearly 60% weight reduction and 40% loss reduction.

The optimal design is then prototyped by joining a 3-turns copper coil in series with a 5-turns aluminum coil in the same slot as shown in Fig. 39. The aluminum coil is placed on top of the copper one to limit the eddy current losses near the slot opening. Finally, the losses in the hybrid coil are measured at different frequencies and compared with those in the full

- Using flat solid coils is the perfect option at low frequency up to 700 Hz, which is the typical range for many types of electrical machines.
- Above 700 Hz, a multi-strand wire with 10 thick strands can have a remarkably better performance up to 1500 Hz.
- Above 1500 Hz, lower loss levels can be realized by using 45 thin strands coils with horizontally-arranged conductors and only one conductor per layer.
- The 45-strand coil with vertical arrangement can be used at very high frequencies (i.e. above 5 kHz) for other types of applications such as high frequency wireless charging.

Thirdly, in terms of materials:

- Due to its higher resistivity, using aluminum instead of copper near the slot opening can limit the AC losses.
- The hybrid coil combines the low losses with low weight and cost. So, it is the optimal choice at high frequency domain for high speed electric drivetrains.

Finally, many factors can affect the selection of magnet wire for electrical machines depending on the application requirements such as frequency, wire flexibility, production time, weight, and cost, or compact structure. So, when it comes down to selection of wire, each option offers distinct advantages in particular scenarios.

APPENDIX

In order to perform the AC loss measurements at a defined temperature value, a specially designed cooling jacket is used with a water chiller to maintain the temperature at a constant level, as shown in Fig. 41.
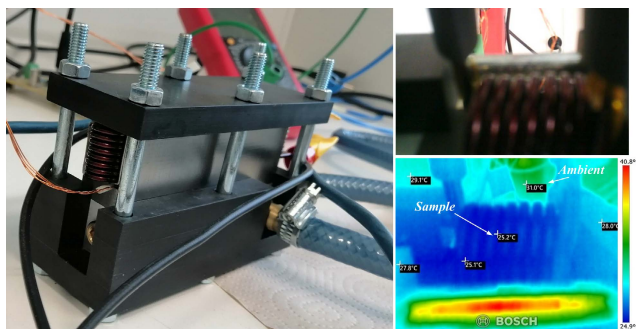

FIGURE 41. Assembly of a test sample with a cooling jacket for temperature control.

ACKNOWLEDGMENT

REFERENCES

[1] A. Selema, M. N. Ibrahim, R. Sprangers, and P. Sergeant, "Effect of using different types of magnet wires on the AC losses of electrical machine windings," in *Proc. IEEE Int. Electr. Mach. Drives Conf. (IEMDC)*, May 2021, pp. 1–5.

[2] Y. Amara, P. Reghem, and G. Barakat, "Analytical prediction of eddy-current loss in armature windings of permanent magnet brushless AC machines," *IEEE Trans. Magn.*, vol. 46, no. 8, pp. 3481–3484, Aug. 2010, doi: 10.1109/TMAG.2010.2046885.

[3] S. Iwasaki, R. P. Deodhar, Y. Liu, A. Pride, Z. Q. Zhu, and J. J. Bremner, "Influence of PWM on the proximity loss in permanent-magnet brushless AC machines," *IEEE Trans. Ind. Appl.*, vol. 45, no. 4, pp. 1359–1367, Jul. 2009, doi: 10.1109/TIA.2009.2023488.

[4] A. Bardalai, X. Zhang, T. Zou, D. Gerada, J. Li, and C. Gerada, "Comparative analysis of AC losses with round magnet wire and Litz wire winding of a high–speed PM machine," in *Proc. 22nd Int. Conf. Electr. Mach. Syst. (ICEMS)*, Aug. 2019, pp. 1–5, doi: 10.1109/ICEMS.2019.8922173.

[5] S. Zhu, K. Paciura, and R. Barden, "Application of flat rectangular wire concentrated winding for AC loss reduction in electrical machines," in *Proc. IEEE Energy Convers. Congr. Expo. (ECCE)*, Oct. 2021, pp. 4619–4623, doi: 10.1109/ECCE47101.2021.9595683.

[6] S. Silber, B. Wex, and K. Kaspar, "Efficient method for simulation of AC losses in permanent magnet synchronous machines," in *Proc. 10th Int. Electr. Drives Prod. Conf. (EDPC)*, Dec. 2020, pp. 1–5, doi: 10.1109/EDPC51184.2020.9388190.

[7] A. Bardalai, D. Gerada, Z. Xu, and C. Gerada, "AC loss analysis in winding of electrical machines with varying strands-in-hand and bundle shapes," in *Proc. 23rd Int. Conf. Electr. Mach. Syst. (ICEMS)*, Nov. 2020, pp. 845–850.

[8] G. Artetxe, B. Prieto, D. Caballero, I. Elosegui, and G. M. Maza, "A practical approach for estimating bundle-level proximity losses in AC machines," *IEEE Trans. Ind. Electron.*, vol. 69, no. 12, pp. 12173–12181, Dec. 2022, doi: 10.1109/TIE.2021.3130348.

[9] G. Du, W. Ye, Y. Zhang, L. Wang, T. Pu, and N. Huang, "Comprehensive analysis of the AC copper loss for high speed PM machine with form-wound windings," *IEEE Access*, vol. 10, pp. 9036–9047, 2022, doi: 10.1109/ACCESS.2022.3143817.

[10] S. G. Min, "Modeling, investigation, and minimization of AC winding loss in slotless PM machines," *IEEE Trans. Energy Convers.*, vol. 36, no. 3, pp. 2249–2260, Sep. 2021, doi: 10.1109/TEC.2021.3050251.

[11] T. Xiao, J. Li, K. Yang, J. Lai, and Y. Lu, "Study on AC copper losses in an air-cored axial flux permanent magnet electrical machine with flat wires," *IEEE Trans. Ind. Electron.*, vol. 69, no. 12, pp. 13255–13264, Dec. 2022, doi: 10.1109/TIE.2022.3144589.

[12] G. Friedman and I. D. Mayergoyz, "On the estimate of eddy current losses in current carrying conductors," *J. Appl. Phys.*, vol. 87, no. 9, pp. 6926–6928, May 2000, doi: 10.1063/1.372588.

[13] P. B. Reddy, T. M. Jahns, and T. P. Bohn, "Modeling and analysis of proximity losses in high-speed surface permanent magnet machines with concentrated windings," in *Proc. IEEE Energy Convers. Congr. Expo.*, Sep. 2010, pp. 996–1003.

[14] M. Spang and M. Albach, "Optimized winding layout for minimized proximity losses in coils with rod cores," *IEEE Trans. Magn.*, vol. 44, no. 7, pp. 1815–1821, Jul. 2008, doi: 10.1109/TMAG.2008.920149.

[15] M. Albach and H. Rossmanith, "The influence of air gap size and winding position on the proximity losses in high frequency transformers," in *Proc. IEEE 32nd Annu. Power Electron. Spec. Conf.*, Jun. 2001, pp. 1485–1490, doi: 10.1109/PESC.2001.954329.

[16] C. R. Sullivan, "Computationally efficient winding loss calculation with multiple windings, arbitrary waveforms, and two-dimensional or three-dimensional field geometry," *IEEE Trans. Power Electron.*, vol. 16, no. 1, pp. 142–150, Jan. 2001, doi: 10.1109/63.903999.

[17] P. B. Reddy, Z. Q. Zhu, S.-H. Han, and T. M. Jahns, "Strand-level proximity losses in PM machines designed for high-speed operation," in *Proc. 18th Int. Conf. Electr. Mach.*, Sep. 2008, pp. 1–6, doi: 10.1109/ICELMACH.2008.4800172.

[18] A. G. Kladas and J. A. Tegopoulos, "Eddy currents modeling in solid iron by using analytic elements," *IEEE Trans. Magn.*, vol. 30, no. 5, pp. 3040–3043, Sep. 1994, doi: 10.1109/20.312578.

[19] P. Mellor, R. Wrobel, and N. McNeill, "Investigation of proximity losses in a high speed brushless permanent magnet motor," in *Proc. Conf. Rec. IEEE Ind. Appl. Conf. 41st IAS Annu. Meeting*, Oct. 2006, pp. 1514–1518, doi: 10.1109/IAS.2006.256730.

[20] J.-H. Choi, Y.-D. Chun, P.-W. Han, M.-J. Kim, D.-H. Koo, J. Lee, and J.-S. Chun, "Design of high power permanent magnet motor with segment rectangular copper wire and closed slot opening on electric vehicles," *IEEE Trans. Magn.*, vol. 46, no. 6, pp. 2070–2073, Jun. 2010, doi: 10.1109/TMAG.2010.2041908.

[21] E. Preci, G. Valente, A. Bardalai, T. Transi, T. Zou, D. Gerada, M. Degano, G. Buticchi, and C. Gerada, "Rectangular and random conductors: AC losses evaluations and manufacturing considerations," in *Proc. IECON 46th Annu. Conf. IEEE Ind. Electron. Soc.*, Oct. 2020, pp. 1076–1081, doi: 10.1109/IECON43393.2020.9254278.

[22] O. Bihler. (2019). *Efficient Automation Solutions for E-Components*. Otto Bihler Maschinenfabrik GmbH, Halblech, Ger. Accessed: Nov. 6, 2021. [Online]. Available: https://meet.bihler.de/en/e-mobility-whitepaper/

[23] (2020). IStock. *Electric Motor Stator Winding*. IStock, Fr. Accessed: Nov. 7, 2021. [Online]. Available: https://www.istockphoto.com/fr/photos/electric-motor-stator-winding-and-stack-close-up

[24] (2019). Elektrisola. *Extruded Litz Wire*. ELEKTRISOLA Dr. Gerd Schildbach GmbH Co KG, Reichshof-Eckenhagen. Accessed: Nov. 10, 2021. [Online]. Available: https://www.elektrisola.com/en-us/Products/Litz-Wire/Products/Extruded

[25] (2019). Elektrisola. *Profiled Litz Wire*. ELEKTRISOLA Dr. Gerd Schildbach GmbH Co KG, Reichshof-Eckenhagen, Ger. Accessed: Nov. 10, 2021. [Online]. Available: https://www.elektrisola.com/en-us/Products/Litz-Wire/Products/Profiled

[26] S. Xue, M. Michon, M. Popescu, and G. Volpe, "Optimisation of hairpin winding in electric traction motor applications," in *Proc. IEEE Int. Electric Mach. Drives Conf. (IEMDC)*, May 2021, pp. 1–7, doi: 10.1109/IEMDC47953.2021.9449605.

[27] M. Paradkar and J. Böcker, "Analysis of eddy current losses in the stator windings of IPM machines in electric and hybrid electric vehicle applications," in *Proc. 8th IET Int. Conf. Power Electron., Mach. Drives (PEMD)*, 2016, p. 5, doi: 10.1049/cp.2016.0320.

[28] D.-S. Jung, Y.-H. Kim, U.-H. Lee, and H.-D. Lee, "Optimum design of the electric vehicle traction motor using the hairpin winding," in *Proc. IEEE 75th Veh. Technol. Conf. (VTC Spring)*, May 2012, pp. 1–4, doi: 10.1109/VETECS.2012.6240320.

[29] Y. Zhao, D. Li, T. Pei, and R. Qu, "Overview of the rectangular wire windings AC electrical machine," *CES Trans. Electr. Mach. Syst.*, vol. 3, no. 2, pp. 160–169, Jun. 2019, doi: 10.30941/CESTEMS.2019.00022.

[30] M. Aoyama and J. Deng, "Visualization and quantitative evaluation of eddy current loss in bar-wound type permanent magnet synchronous motor for mild-hybrid vehicles," *CES Trans. Electr. Mach. Syst.*, vol. 3, no. 3, pp. 269–278, Sep. 2019, doi: 10.30941/CESTEMS.2019.00035.

[31] R. P. Wojda and M. K. Kazimierczuk, "Winding resistance of litz-wire and multi-strand inductors," *IET Power Electron.*, vol. 5, no. 2, p. 257, 2012, doi: 10.1049/iet-pel.2010.0359.

[32] C. R. Sullivan, "Cost-constrained selection of strand diameter and number in a Litz-wire transformer winding," *IEEE Trans. Power Electron.*, vol. 16, no. 2, pp. 281–288, Mar. 2001, doi: 10.1109/63.911153.

[33] W. Zhao, X. Wang, S. Wu, S. Cui, C. Gerada, and H. Yan, "Eddy current losses analysis and optimization design of Litz-wire windings for air-core compulsators," *IEEE Trans. Plasma Sci.*, vol. 47, no. 5, pp. 2532–2538, May 2019, doi: 10.1109/TPS.2019.2901628.

[34] A. Dannier, F. Di Bruno, F. Fiume, E. Fedele, and G. Brando, "Hairpin winding technology for electric traction motors: Design, prototyping, and connection rules," in *Proc. Int. Conf. Electr. Mach. (ICEM)*, Sep. 2022, pp. 1170–1175, doi: 10.1109/ICEM51905.2022.9910851.

[35] A. Bardalai, D. Gerada, D. Golovanov, Z. Xu, X. Zhang, J. Li, H. Zhang, and C. Gerada, "Reduction of winding AC losses by accurate conductor placement in high frequency electrical machines," *IEEE Trans. Ind. Appl.*, vol. 56, no. 1, pp. 183–193, Jan. 2020, doi: 10.1109/TIA.2019.2947552.

[36] A. Selema, D. S. M. Osheba, S. M. R. Tahoon, and M. M. El-Shanawany, "Design and analysis of a three-phase brushless flux switching generator for aircraft ground power units," *IET Electr. Power Appl.*, vol. 13, no. 2, pp. 154–161, Feb. 2019, doi: 10.1049/iet-epa.2018.5307.

[37] A. Tenconi, S. Vaschetto, and A. Vigliani, "Electrical machines for high-speed applications: Design considerations and tradeoffs," *IEEE Trans. Ind. Electron.*, vol. 61, no. 6, pp. 3022–3029, Jun. 2014.

[38] M. A. Rahman, A. Chiba, and T. Fukao, "Super high speed electrical machines–summary," in *Proc. IEEE Power Eng. Soc. Gen. Meeting*, Jun. 2004, pp. 1272–1275.

[39] A. Ridge, K. K. Ahamad, R. Mcmahon, and J. Miles, "Development of a 50 kW wireless power transfer system," in *Proc. IEEE PELS Workshop Emerg. Technol., Wireless Power Transf. (WoW)*, Jun. 2019, pp. 406–409.

AHMED SELEMA (Member, IEEE) received the M.Sc. degree in electrical engineering from Menoufia University, Egypt, in 2018. He is currently pursuing the Ph.D. degree with the Department of Electromechanical, Systems and Metal Engineering, Ghent University, Belgium. He has been also working as a Research Engineer with the Electrical Energy Laboratory (EELab), Ghent University, in a close collaboration with different industrial corporations in the EU. His research interests include electrical machines and drives, electromagnetics, material characterization, energy-efficient motor design, machines losses and cooling, and additive manufacturing. In these areas, he has authored or coauthored many articles in leading journals.

MEHMET GULEC received the M.Sc. and Ph.D. degrees in mechatronics engineering from Kocaeli University, Kocaeli, Turkey, in 2013 and 2019, respectively. From 2017 to 2018, he was a Scholarship Holder of the Finnish Government for doctoral study with LUT University, Lappeenranta, Finland. He is currently a Postdoctoral Researcher with the Department of Electromechanical, Systems and Metal Engineering, Ghent University, Ghent, Belgium. His current research interests include modeling, design, and optimization of e-motors for hybrid and electric vehicles.

MOHAMED N. IBRAHIM received the M.Sc. degree in electrical power and machines engineering from Tanta University, Egypt, in 2012, and the Ph.D. degree in electromechanical engineering from Ghent University, Belgium, in 2017. He is currently working as a Postdoctoral Researcher with the Department of Electromechanical, Systems, and Metal Engineering, Ghent University. He is also an Assistant Professor (on leave) with the Department of Electrical Engineering, Kafrelshiekh University. He is also an Affiliate Member of Flanders Make, the strategic research center for the manufacturing industry in Flanders, Belgium. His major research interests include design and control of electrical machines and drives for industrial and sustainable energy applications. He also serves as a reviewer and a guest editor for several journals.

RUUD SPRANGERS received the M.Sc. and Ph.D. degrees (*cum laude*) from the Eindhoven University of Technology, in 2011 and 2015, respectively. He is currently working as an Advanced Technology Engineer at Punch Powertrain. His research interests include design and analysis of electric machines, and in particular on the application of new and emerging materials and technologies within such machines. This also includes the development and validation of an automated optimization platform for industrial electric motors.

PETER SERGEANT (Senior Member, IEEE) received the M.Sc. degree in electromechanical engineering and the Ph.D. degree in engineering sciences from Ghent University, Ghent, Belgium, in 2001 and 2006, respectively. He became a Postdoctoral Researcher at Ghent University, in 2006 (Postdoctoral Fellow of the Research Foundation-Flanders). Since 2012, he has been an Associate Professor at Ghent University. He is currently a Professor of electrical drives at Ghent University and a Core Laboratory Manager in the cluster motion products of Flanders Make. His current research interests include electrical machines and drives for industrial and sustainable energy applications.

● ● ●